METALS

Lowering coefficient of friction in Cu alloys with stable gradient nanostructures

Xiang Chen,* Zhong Han,* Xiuyan Li,* K. Lu†

The coefficient of friction (COF) of metals is usually high, primarily because frictional contacts induce plastic deformation underneath the wear surface, resulting in surface roughening and formation of delaminating tribolayers. Lowering the COF of metals is crucial for improving the reliability and efficiency of metal contacts in engineering applications but is technically challenging. Refining the metals' grains to nanoscale cannot reduce dry-sliding COFs, although their hardness may be elevated many times. We report that a submillimeter-thick stable gradient nanograined surface layer enables a significant reduction in the COF of a Cu alloy under high-load dry sliding, from 0.64 (coarse-grained samples) to 0.29, which is smaller than the COFs of many ceramics. The unprecedented stable low COF stems from effective suppression of sliding-induced surface roughening and formation of delaminating tribolayer, owing to the stable gradient nanostructures that can accommodate large plastic strains under repeated sliding for more than 30,000 cycles.

INTRODUCTION

In contrast to ceramics and polymers, most metals exhibit high coefficients of friction (COFs) under dry sliding, generally ranging from 0.6 to 1.2 in the steady state (*1*, *2*). Sliding-induced plastic deformation and subsequent microstructure changes underneath the wear surface are believed to be responsible for metals' high COFs. During sliding, local asperity contacts cause accumulated plastic straining that makes the near-surface material susceptible to shear instabilities (*3*), triggering surface roughening by microcracking or folding that elevates the mechanical component (for example, ploughing) of the COF. Repeated sliding on the roughened surface generates wear particles, leading to mechanical alloying and cold welding of the particles with the worn surface, forming nanostructured tribolayers (*4*–*7*). Delamination of the brittle tribolayers in subsequent sliding leads to further surface roughening and high COF.

Although it is technically challenging, lowering the COFs of metals under dry sliding is of great technological significance for improving the reliability and efficiency of metal contacts in engineering applications ranging from heavy-load gears to mining and rolling machines. Refining the metals' grains into nanoscale was expected to reduce the COFs because it elevates the hardness many times. Lower COFs were indeed observed in a few nanograined (NG) metals under "gentle" sliding (*8*, *9*), that is, at low sliding speeds and/or forces or with lubrication. However, for many metals [Ni (*9*), Ti (*10*), Al (*11*), and Cu (*12*)] and alloys (*13*–*16*), no reduction in COF was observed in their NG states compared with their coarse-grained (CG) counterparts under high-load (or speed) sliding, even with lubrication. This originates from the very limited plastic deformation ability of NG structures in which strain localization is induced by high-load sliding (*16*), leading to surface roughening and delamination. Clear correspondences between high COFs and the formation of delaminating tribolayers were observed in NG metals (*8*).

Finishing or polishing processes are known to form a very thin nanostructured layer on metal surfaces. This submicrometer-thick nanostructured layer may considerably reduce the COF under lubricated sliding with gentle run-in conditions (*17*, *18*), but COF reduction disappeared at high sliding speeds (*17*). The friction-induced nanostructured layer is ineffective in lowering the COFs under dry sliding (*7*, *8*, *19*, *20*), during which the sliding-induced plastic deformation is much more intensive than that with lubrication. This phenomenon also stems from the mechanical instability of the thin nanostructured layer and its tendency to form delaminating tribolayers under dry sliding, which is analogous to that in bulk NG metals. Therefore, to lower the dry-sliding COFs of metals, it is necessary to increase the stability of the subsurface nanostructures against sliding-induced plastic deformation so that surface roughening and formation of delaminating tribolayers can be suppressed.

By controlling a newly developed surface mechanical grinding treatment (SMGT), a gradient nanograined (GNG) surface layer with a thickness in millimeter scale can be produced on various metals and alloys, in which grain sizes increase gradually from tens of nanometers in the top surface to micrometers in the interior. This thick GNG layer is mechanically stable, capable of suppressing strain localization and accommodating very large plastic strains before failure under tension (*21*, *22*). Here, we studied the effect of this stable GNG surface layer on the dry-sliding COF in a Cu-Ag alloy. Reduced steady-state COF is obtained under high-load sliding with substantial plastic deformation in the surface layer, owing to the successful suppression of the sliding-induced surface roughening and delaminating with the GNG structures.

RESULTS AND DISCUSSION

A depth-dependent GNG structure was generated in a bulk CG Cu-Ag [5 weight % (wt %)] alloy rod by SMGT (Fig. 1A). Ag is added to stabilize the deformed structure against recrystallization during SMGT. The topmost surface layer is characterized by roughly equiaxed and randomly oriented nanograins (Fig. 1B) with an average transversal size of 25 nm. Grains become larger as the depth increases while maintaining their random orientations. The average sizes reach about 100 nm at a depth of 80 μm (Fig. 1C). Deeper than 150 μm are typical deformation structures including dislocation cells and subgrains with sizes in the submicrometer or micrometer scale. The total thickness of deformation structures is about 0.7 mm. A microhardness gradient ranging from 2.9 GPa at the surface to 0.85 GPa corresponds to the grain size gradient (Fig. 1C).

COFs of the GNG samples were measured by means of an oscillating friction and wear tester in ball-on-plate contact configuration using a WC-Co ball (10 mm in diameter) with a load of 50 N and a

Shenyang National Laboratory for Materials Science, Institute of Metal Research, Chinese Academy of Sciences, Shenyang 110016, China.
*These authors contributed equally to this work.
†Corresponding author. Email: lu@imr.ac.cn

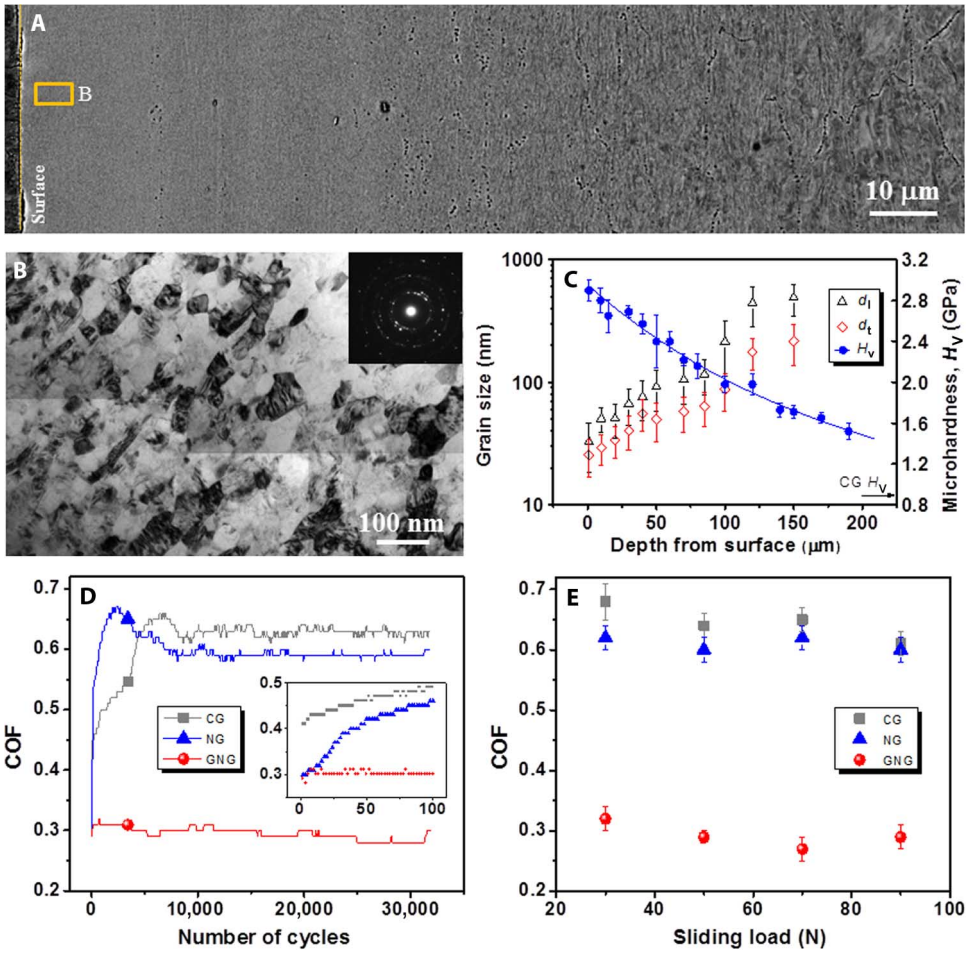

Fig. 1. GNG structure and COF in the Cu-Ag sample. (**A**) Typical longitudinal-sectional scanning electron microscopy image of the as-prepared GNG Cu-Ag sample. (**B**) Bright-field TEM image about 3 μm below the surface in (A); inset shows a corresponding electron diffraction pattern. (**C**) Variation of longitudinal (d_l) and transversal grain sizes (d_t) and microhardness along depth from the surface. Error bars represent the SD of grain size and hardness measurements. (**D**) Variation of COFs with sliding cycles for the CG, NG, and GNG Cu-Ag samples sliding against WC-Co balls under a load of 50 N, a slide stroke of 1 mm, and a velocity of 10 mm/s. Inset shows COFs during the initial 100 cycles. (**E**) Variations of the steady-state COFs with the applied load for the three samples.

slide stroke of 1.0 mm at a speed of 10 mm/s. For comparison, CG (20 μm in grain size) and NG Cu-5Ag samples were measured under the same conditions. The NG sample prepared using dynamic plastic deformation (DPD) is structurally characterized by nanosized grains (averagely 60 nm in size) mixed with a small fraction of nanotwinned (about 22 nm in twin thickness) regions. It exhibits a microhardness of 2.4 ± 0.5 GPa, close to that in the GNG surface layer. X-ray diffraction and transmission electron microscopy (TEM) analyses indicated that both the GNG surface layer and the NG samples have a single Cu phase without detectable Ag precipitation. It implies that Ag may exist in Cu NGs or boundaries or in the form of extremely fine Ag particles, which are too small to be detected in both samples. The maximum Hertzian contact stress under a load of 50 N was estimated to be about 1.78 GPa, which far exceeds the yield strength of the GNG surface layer and the NG samples, respectively, implying that substantial plastic deformation is imposed in their surface layers. Before sliding, the three samples were electrochemically polished to the same level of surface roughness (R_a < 0.03 μm and R_z < 0.18 μm).

The measured COF of the CG samples increases immediately upon sliding, from 0.41 to 0.49 at 100 cycles (Fig. 1D). It tends to a steady state at 0.64 after several thousand cycles, a typical frictional response of metals with consistent COF values, as reported in the literature (*2*). A similar COF variation was seen in the NG sample: It rises from 0.30 to 0.46 at 100 cycles, approaching a steady state at 0.60 with further sliding, comparable to that of the CG. This behavior agrees with that in other NG materials under high-load sliding (*8*). For the GNG sample, the initial COF is 0.30, which is comparable to the NG value. However, the COF remains unchanged with increasing sliding, even after more than 30,000 cycles. Repeated measurements with at least five tests for each sample (fig. S1) showed that the steady-state COFs of the GNG samples change slightly from 0.25 to 0.32 with an increasing load from 30 to 90 N (averagely 0.29; Fig. 1E), much lower than the COFs of the NG and CG samples (0.60 to 0.68). This low steady-state COF is even smaller than that of many ceramics under dry sliding (*1*). The measured wear volume of the GNG sample sliding for 27,000 cycles under a load of 50 N is 2.5×10^6 μm^3, much smaller than that in the NG (1.2×10^7 μm^3) and CG (2.6×10^7 μm^3) samples (fig. S2). The corresponding wear rate for the GNG sample (9.35×10^{-7} mm^3/Nm) is also much smaller than that of the NG (4.4×10^{-6} mm^3/Nm) and CG (9.6×10^{-6} mm^3/Nm) samples, respectively.

We investigated surface morphology and roughness variation during sliding to understand the COF difference. After a single one-way

sliding on the CG sample at a load of 50 N, a 2.2-μm-deep scar was generated, in which small cracks and pileups of submicrometer heights/depths and micrometer lengths appeared (Fig. 2A). Most of them are perpendicular to the sliding direction. Similar surface roughening behaviors were observed at lower sliding loads with smaller scars (about 1 μm deep) but with a smaller density and depth of cracks (fig. S3). The formation of pileups and cracks after a single sliding indicates that the sliding-induced plastic strain in the surface layer is too large to be accommodated. This observation echoes a recent measurement in Al wherein a single sliding is sufficient to damage the surface, forming crack-like features and surface tears (*23*).

A single sliding on the NG sample under the same conditions caused a smaller scar 0.7 μm deep due to its high hardness, while surface roughening appeared too. Microsized cracks and pileups were induced by a single sliding (Fig. 2A). The density of cracks is smaller, but their length is larger compared with those in the CG sample. Crack/pileup formation is understandable with large plastic strains imposed in the NG surface layer with very limited plastic deformability.

The GNG sample shows a distinct scenario. Under the same sliding conditions, a scar about 0.7 μm deep was formed after a single sliding, indicating a comparable surface hardness to that of the NG sample, but the scar surface was smooth without any crack or pileup (Fig. 2A). The surface roughness along the sliding direction was identical to that of the original sample, which indicated that the sliding-induced plastic strain was well accommodated by the GNG structure without generating strain localization.

After multiple repeated sliding, the density and sizes (both in length and depth/height) of the surface cracks/pileups increased in the CG and NG samples (Fig. 2B). Surface roughness increased in the first 100 cycles to R_a = 0.08 μm for both CG and NG samples, and R_z = 0.8 and 0.6 μm for CG and NG samples, respectively (Fig. 3A). Larger R_z values in the CG resulted from larger plastic strains imposed on the surface layer with a deeper scar. After a few thousand cycles into the steady state, the surfaces become even rougher (Fig. 2B), with a steady roughness of R_a = 0.2 μm and R_z = 2.0 μm for both samples. However, for the GNG sample, no crack or pileup was detected after multiple sliding. The sliding surface remained essentially as smooth as the original even after 30,000 cycles (Fig. 2B), and the measured roughness was $R_a = 0.02 \pm 0.011$ μm and $R_z = 0.1 \pm 0.03$ μm, identical to the original (table S1). This result indicated that the sliding-induced surface roughening was suppressed in the GNG sample, fundamentally distinct from that in the homogeneous NG and CG samples.

Pure Cu samples with a similar GNG surface layer without Ag addition showed exactly the same surface nonroughening behaviors with

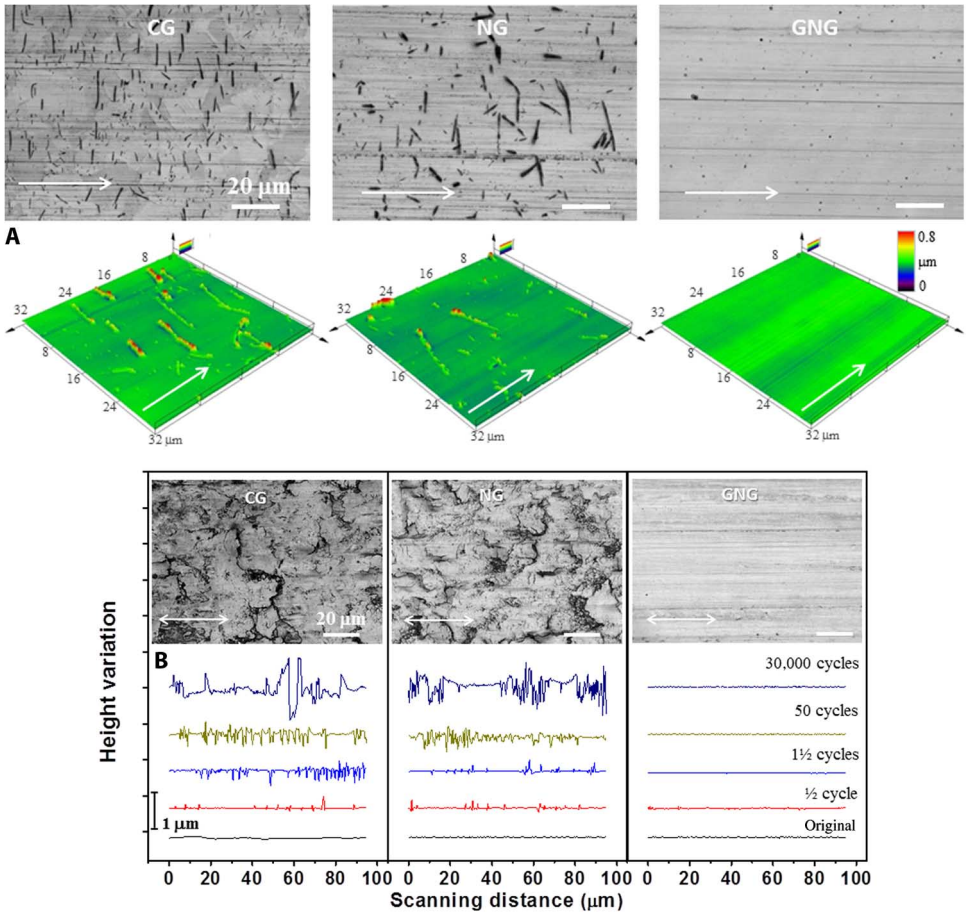

Fig. 2. Surface morphology after a single and repeated sliding. (**A**) Confocal laser microscopy images and 3D profiles for surface morphologies of the CG, NG, and GNG Cu-Ag samples after a single sliding. White arrows indicate the sliding directions. (**B**) Measured surface height profiles along the sliding direction in the CG, NG, and GNG Cu-Ag samples after different sliding cycles (as indicated), with corresponding confocal laser microscopy images for surface morphologies after sliding for 18,000 cycles (above). A load of 50 N, a slide stroke of 1 mm, and a velocity of 10 mm/s were applied for each sample. White double-ended arrows indicate the sliding directions.

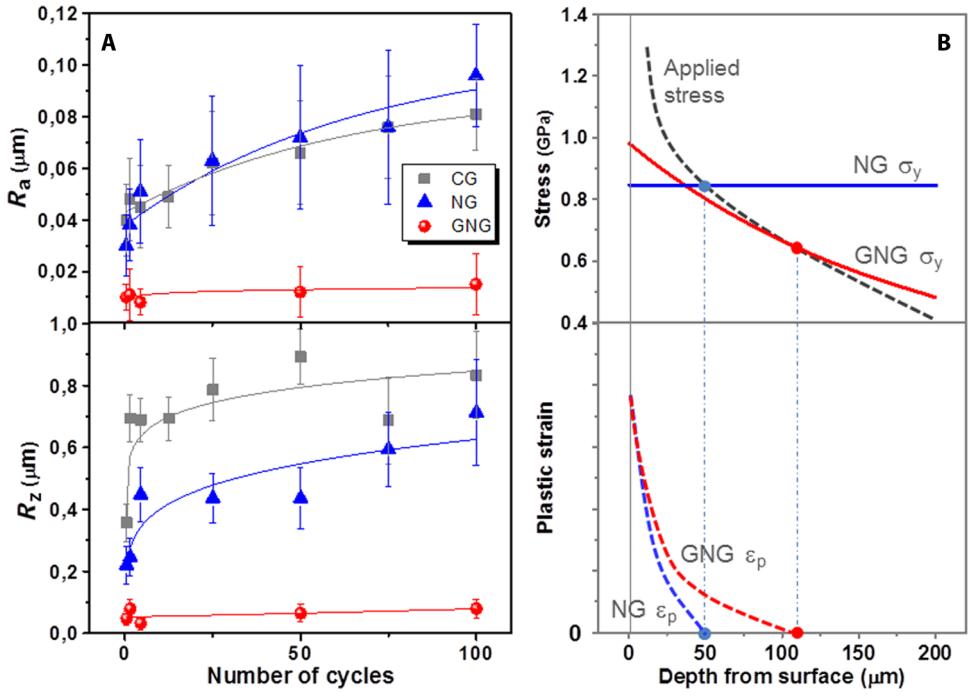

Fig. 3. Variation of surface roughness and plastic strain gradients in the GNG and homogeneous NG samples. (**A**) Variations of average surface roughness (R_a and R_z) along the sliding direction with number of cycles in the CG, NG, and GNG samples. (**B**) Schematic variations of applied stress (dashed line, above) and plastic strain (ε_p; dashed lines, below) along the depth from the sliding surface in the GNG and NG samples, respectively. Measured variations of yield strength along the depth for the GNG (taken as approximately one-third microhardness) and NG samples are included (σ_y; solid lines). The depth of plastic deformation for the two samples was determined from subsurface structural observations.

a much reduced COF (0.37) under dry sliding for several thousand cycles. In comparison, the pure Cu NG and CG samples exhibit high steady-state COF values (0.66 and 0.75, respectively) with immediate surface roughening under the same sliding conditions (fig. S4). Apparently, the observed surface nonroughening and COF reduction are not a result of Ag addition. Microstructure characterization combined with surface chemical analysis indicated no transfer layer on the WC-Co ball surfaces after the dry-sliding tests for each sample. The chemical compositions of the counter surface are essentially identical after sliding for 18,000 cycles for the three samples (fig. S5), implying that the counter surface effect on the COF difference can be excluded. This is verified by switching the COF measurements among the CG, NG, and GNG samples (fig. S6).

Suppression of sliding-induced surface roughening stems from the unique GNG surface layer. For the homogeneous NG sample, the elastic limit from the surface to the interior is identical. On a contact load, plastic strains are imposed only on the top surface layer where the local stress exceeds the elastic limit, which drops to zero at a small depth (Fig. 3B). This means that plastic deformation is concentrated in a thin surface layer with a large strain gradient along the depth, likely inducing strain localization and surface cracking even after a single sliding, as observed in Fig. 2A. Repeated sliding on the cracked surface may detach the crack-like features, generate particles, and cold-weld them onto the surface again, eventually forming a nanostructured tribolayer. The formation of the brittle tribolayer that delaminates during sliding is responsible for the high COF and surface roughness (*8*), as supported by the correlating variations of surface roughness (Fig. 3A) and those of the COF (Fig. 1D).

For the GNG sample, a gradient in the elastic limit is inherent. Upon contact loading, plastic deformation may be initiated within a thick surface layer in which the local stress exceeds the elastic limits, which drop with an increasing depth, generating a much smaller gradient in plastic strain than in the homogeneous NG sample (Fig. 3B). Subsurface structural observations showed that the layer depth that has undergone plastic deformation is obviously larger in the GNG sample (100 to 150 μm) than in the NG one (40 to 50 μm; Fig. 3B). Hence, strain localization in the sliding surface can be effectively released so that surface deformation instability is suppressed. This argument is verified by the cross-sectional TEM observations that the GNG structure is very stable against plastic deformation under repeated high-load sliding, which explains the surface nonroughening and the stable low COF observed in the GNG samples.

Cross-sectional TEM observations of the worn subsurface GNG layer showed that after sliding for a few hundred cycles, no obvious structural change was noticed in the topmost layer (<0.5 μm thick) consisting of randomly oriented NGs with an average size of ~30 nm (comparable to the original size). Underneath the topmost layer, coarsening of NGs occurred, with increased average sizes to about 130 nm in a depth span of 0.5 to 2 μm. No obvious grain coarsening is seen at a larger depth. This subsurface structure remains very stable with increasing sliding cycles to as much as 27,000: the topmost layer persists with stable thickness and grain sizes; the grain-coarsened layer thickens slightly and saturates at a few micrometers, with grain sizes in the submicrometer scale (Fig. 4A and fig. S7). The high stability of the subsurface structure against repeated sliding can also be seen from the measured grain size profiles along the depth with increasing sliding cycles (Fig. 4B). Measured grain sizes are close to the original values as the depth exceeds 40 μm because of decreased strains. Grain coarsening in the subsurface layer is dominated by a mechanically driven grain boundary process (*21*, *24*–*26*). A dynamic saturation in microstructures in the

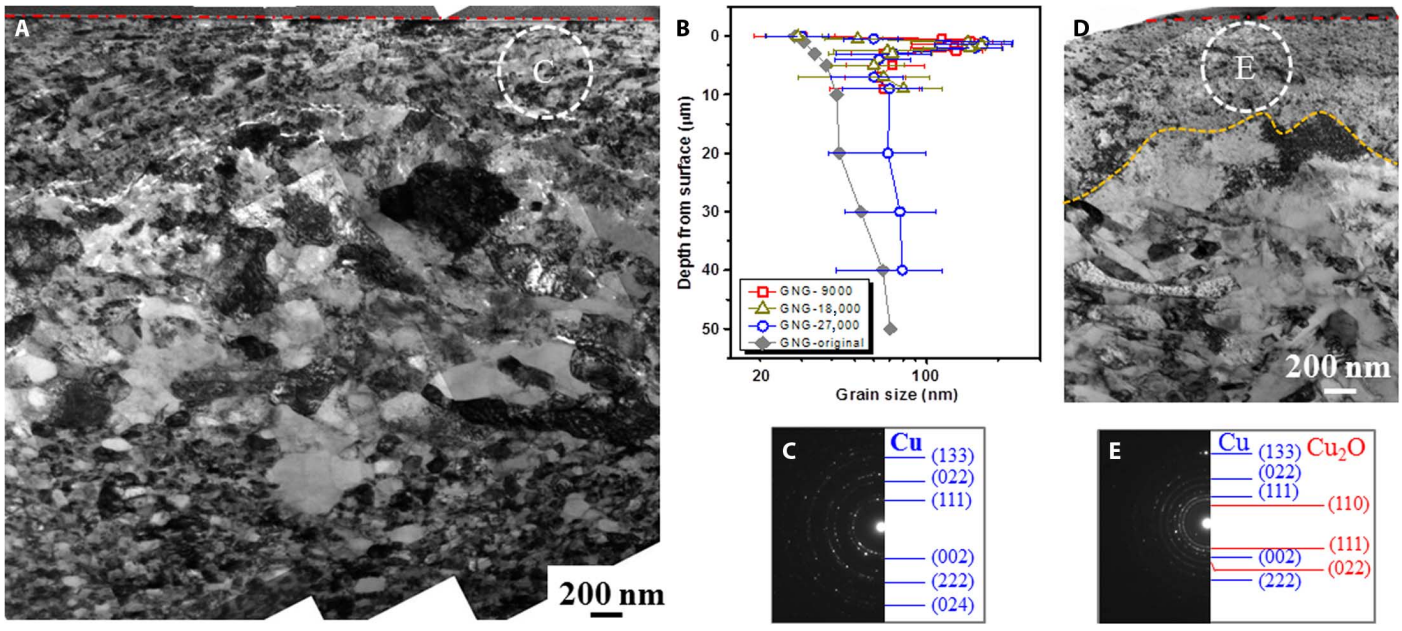

Fig. 4. Friction-induced subsurface microstructure evolution. (**A**) Typical cross-sectional TEM image of the subsurface layer in the GNG sample after sliding for 27,000 cycles. (**B**) Variation of the mean grain sizes along the depth determined from TEM images in the GNG samples before and after sliding for 9000, 18,000, and 27,000 cycles, respectively. (**C**) Corresponding electron diffraction pattern in the topmost surface layers [as indicated in (A)]. (**D**) Typical cross-sectional TEM image of the subsurface layer in the NG samples after sliding for 18,000 cycles. (**E**) Corresponding electron diffraction pattern in the topmost surface layers [as indicated in (D)]. Sliding surfaces are outlined by dash-dotted lines, and the tribolayer/recrystallization interfaces by dashed lines. A load of 50 N, a slide stroke of 1 mm, and a velocity of 10 mm/s were applied for each sample.

submicrometer scale is reached when the manipulation of dislocations and grain boundaries is balanced with the grain boundary migration process accompanied with dislocation annihilation, as is usually observed in the severe plastic deformation of metals (*27*, *28*). Hence, the submicrometer-sized structures remained stable with increasing straining.

Electron diffraction and chemical composition analysis using energy-dispersive x-ray spectroscopy scanning were performed on the 0.5-μm topmost layer, which exhibited extraordinary stability against repeated sliding, as subjected to very large shear strains and strain gradients. No oxides or other phases except pure Cu were found (Fig. 4C), and the composition distributions of Ag and Cu are very homogeneous across the layer without measurable impurities including oxygen (fig. S8). Similar subsurface structures were observed in other NG samples with low COFs under gentle sliding (*8*, *9*). A very high density of geometrically necessary dislocation might be imposed in terms of the strain gradient plasticity theory (*29*), associating with surface-mediated dislocation activities as surfaces provide copious dislocation sources and sinks. Grain boundary–mediated processes may also play a crucial role in stabilizing the extremely fine NG structures (*16*). However, the detailed plastic deformation mechanism and the extraordinary stability of this topmost layer need further clarification with more in-depth investigations.

The NG sample has a different worn subsurface structure in the steady state (Fig. 4D) but is very similar to that in the CG samples (fig. S8). A nanostructured tribolayer containing a few nanometer-sized Cu_2O and Cu grains developed rapidly in the initial sliding stage. It thickens with increasing cycles tending to a steady thickness of several micrometers, which corresponds to the low-to-high COF transition, consistent with the literature (*8*). Plenty of cracks are identified in the brittle tribolayer and along interfaces between the tribolayer and recrystallization (fig. S9), indicating the delamination and wear-off tendency of the tribolayer in subsequent sliding. Underneath the tribolayer are dynamic recrystallization structures containing randomly oriented submicrometer-sized grains (averagely 200 nm), as usually seen in Cu and Cu alloys (*7*, *30*). The original nanostructures are deeper than about 40 to 50 μm.

In comparison, one may find a distinct feature of the worn subsurface structures in the GNG sample: a continuous submicrometer-thick topmost layer consisting of nanosized grains without any inclusions of oxide particles, rather than a tribolayer. It attaches on a CG layer, and between them is a gradient change in grain sizes. This elastically homogeneous but plastically gradient subsurface structure exhibits a superior stability against contact loading, which involves a gradient distribution of stress. Hence, the subsurface structures remain stable during repeated sliding, maintaining high smoothness. In contrast, in the NG and CG samples, a micrometer-thick tribolayer with extremely fine nanostructures is formed atop a recrystallized layer with submicrosized grains, and between them is a distinct interface with a sharp change in grain size and chemical constitution. The brittle tribolayers are easy to delaminate, causing surface roughening.

CONCLUSIONS

The superior stability of the intentionally made GNG structure against sliding-induced surface roughening and delamination provides a novel strategy for enhancing friction and wear resistance of metals and alloys. Similar behaviors of obvious COF reduction and wear resistance enhancement with the stable GNG surface layers have been observed in other materials including pure copper and stainless steels. Therefore, the finding is generally significant and may find tremendous potential for technological applications in contact loading of metals.

MATERIALS AND METHODS

Sample preparation

A Cu-5Ag (wt %) alloy was prepared by arc melting under high vacuum. After annealing at 1123 K for 2 hours, a homogeneous CG structure with an average grain size of about 20 μm was formed in the Cu-5Ag alloy.

A GNG surface layer was prepared on a CG Cu-5Ag alloy by SMGT (*31*). A cylinder Cu-5Ag bar with a diameter of 15 mm and a length of 100 mm was processed using the SMGT with a hemispherical WC-Co tool tip with a radius of 8 mm at cryogenic temperature (~173 K). The SMGT processing parameters are as follows: the rotating velocity of the sample v_1 = 600 rpm, the sliding velocity of the tool tip v_2 = 3 mm/min, the preset penetration depth of the tool tip into the sample a_p = 40 μm. To increase the plastic strain to achieve a thick GNG layer, we treated the sample using multiple passes with an additional 40 μm in indentation depth in each subsequent pass. The SMGT process was repeated six times with the same processing parameters, and the tip indent depth reached 240 μm in the last treatment. Plastic deformation was rather uniform in the subsurface layer with a small surface roughness ($R_a \approx$ 0.2 μm). No crack was identified in the surface of the SMGT sample.

Bulk NG Cu-5Ag alloy samples were prepared using the DPD technique (*32*). A CG Cu-5Ag cylinder (15 mm in diameter and 20 mm in height) cooled by liquid nitrogen was compressed at a high strain rate (~10^3 s^{-1}). Multiple impacts were applied to deform a cylinder sample eventually to a disc with a thickness of 2.7 mm. The total accumulative strain was about 2.0. The microstructure of the DPD sample consisted of nanosized grains with an average size of about 60 nm mixed with a small fraction of submicrosized regions with nanotwins (twin thickness λ = 22 nm).

Friction tests

Sliding friction tests of the Cu-5Ag samples were performed on an Optimol SRVIII oscillating friction tester in a ball-on-plate contact configuration under dry conditions at room temperature (25°C) in air with a relative humidity of 45%. Balls 10 mm in diameter were made of WC-Co with a microhardness of 17.5 GPa. The GNG samples were cut from the SMGT specimens. The sliding surface was made flat with mechanical and electrochemical polishing. The friction tests were carried out along the length direction of the SMGT bar at a slide stroke of 1 mm; a normal load of 30, 50, 70, and 90 N; and a sliding velocity of 0.01 m/s. One sliding cycle is defined as two strokes. The COF was measured as $\mu = F/P$, where F is the frictional force measured by the tester and P is the normal applied load. The COF values were recorded automatically.

Wear rates of the materials were determined by measuring the profiles of the worn surfaces using a MicroXAM 3D surface profilometer system. A reference surface was determined to quantify the volume of a wear scar, and the volume of materials below the reference surface was taken as the wear volume, including the small pileup volume above the reference surface at the edge of the wear scar. An effective length of 1 mm of wear scar was used for determining the wear volume.

The maximum Hertzian contact pressure σ_{max} was calculated by Eqs. 1 to 3

$$\sigma_{max} = \frac{3P}{2\pi a^2} \quad (1)$$

$$a = \sqrt[3]{\frac{3PR}{4E'}} \quad (2)$$

$$\frac{1}{E'} = \frac{1-\nu_1^2}{E_1} + \frac{1-\nu_2^2}{E_2} \quad (3)$$

where R is the radius of the WC ball, E_1 and E_2 represent the elastic modulus of the ball and plate, and ν_1 and ν_2 represent the Poisson's ratio, respectively. With a Young's modulus of 130 GPa for Cu-Ag and 680 GPa for WC and a Poisson ratio of 0.32 for Cu-Ag and 0.24 for WC, for normal loads of 30, 50, 70, and 90 N, the corresponding Hertzian contact stress was 1.5, 1.78, 1.99, and 2.16 GPa, respectively.

Surface morphology and roughness

Surface morphology and roughness of the Cu-5Ag samples were measured using an Olympus 4000 confocal laser scanning microscope, with a height resolution in z axe of 10 nm.

Structure characterization of wear subsurface

Cross-sectional structural characterization of the wear subsurface layers in these samples was carried out using an FEI Nova NanoSEM 430 system and a JEM-2010 TEM operated at a voltage of 200 kV. The cross-sectional TEM foils of the as-prepared GNG sample were made by electrodepositing a Cu coating (about 1.5 mm thick) on the GNG surface, cutting cross-sectional foils, mechanical polishing, and ion milling using the Gatan precision ion polishing system.

For the worn samples, cross-sectional TEM foils for the characterization of wear subsurface were prepared by cutting at the middle of the wear track parallel to the sliding direction using the standard lift-out method in a focused ion beam (FIB) system (FEI Helios NanoLab DualBeam 650). A thin layer of platinum was deposited on the worn surface for protection against the beam damage. For microstructure characterization at deep subsurface positions, cross-sectional samples were cut perpendicular to the sliding direction in the center of the wear tracks. TEM foils were accurately positioned and prepared using the FIB lift-out method. Similarly, a thin platinum layer was deposited on the sample surfaces for protection.

SUPPLEMENTARY MATERIALS

Supplementary material for this article is available at http://advances.sciencemag.org/cgi/content/full/2/12/e1601942/DC1

fig. S1. Measurement repeatability of COF.
fig. S2. Measurement results of wear rates.
fig. S3. Surface profiles and morphology of the CG sample under low-load single sliding.
fig. S4. Effect of Ag addition on COF reduction—Measurement results in pure Cu samples.
fig. S5. Counter surface analysis.
fig. S6. COF measurement on the NG, GNG, and CG samples subsequently using exactly the same contact surface of a WC-Co ball.
fig. S7. Stability of the subsurface microstructure in the GNG samples against sliding.
fig. S8. Chemical analysis of the topmost NG surface layer.
fig. S9. Subsurface microstructures in the CG Cu under sliding in the steady state.
table S1. Surface roughness change after dry sliding for 18,000 cycles.

REFERENCES AND NOTES

1. F. P. Bowden, D. Tabor, *The Friction and Lubrication of Solids* (Clarendon Press, 1986).
2. J. M. Jungk, J. R. Michael, S. V. Prasad, The role of substrate plasticity on the tribological behavior of diamond-like nanocomposite coatings. *Acta Mater.* **56**, 1956–1966 (2008).
3. D. A. Rigney, Transfer, mixing and associated chemical and mechanical processes during the sliding of ductile materials. *Wear* **245**, 1–9 (2000).
4. H.-J. Kim, S. Karthikeyan, D. Rigney, A simulation study of the mixing, atomic flow and velocity profiles of crystalline materials during sliding. *Wear* **267**, 1130–1136 (2009).
5. D. A. Rigney, S. Karthikeyan, The evolution of tribomaterial during sliding: A brief introduction. *Tribol. Lett.* **39**, 3–7 (2010).

6. J. B. Singh, J.-G. Wen, P. Bellon, Nanoscale characterization of the transfer layer formed during dry sliding of Cu–15 wt.% Ni–8 wt.% Sn bronze alloy. *Acta Mater.* **56**, 3053–3064 (2008).
7. X. Chen, Z. Han, K. Lu, Wear mechanism transition dominated by subsurface recrystallization structure in Cu–Al alloys. *Wear* **320**, 41–50 (2014).
8. H. A. Padilla II, B. L. Boyce, C. C. Battaile, S. V. Prasad, Frictional performance and near-surface evolution of nanocrystalline Ni–Fe as governed by contact stress and sliding velocity. *Wear* **297**, 860–871 (2013).
9. S. V. Prasad, C. C. Battaile, P. G. Kotula, Friction transitions in nanocrystalline nickel. *Scr. Mater.* **64**, 729–732 (2011).
10. M. Wen, C. Wen, P. D. Hodgson, Y. C. Li, Tribological behaviour of pure Ti with a nanocrystalline surface layer under different loads. *Tribol. Lett.* **45**, 59–66 (2012).
11. Z. N. Farhat, Y. Ding, D. O. Northwood, A. T. Alpas, Effect of grain size on friction and wear of nanocrystalline aluminum. *Mater. Sci. Eng. A* **206**, 302–313 (1996).
12. Y. S. Zhang, Z. Han, K. Wang, K. Lu, Friction and wear behaviors of nanocrystalline surface layer of pure copper. *Wear* **260**, 942–948 (2006).
13. X. Chen, Z. Han, K. Lu, Enhancing wear resistance of Cu–Al alloy by controlling subsurface dynamic recrystallization. *Scr. Mater.* **101**, 76–79 (2015).
14. F. Ren, S. N. Arshad, P. Bellon, R. S. Averback, M. Pouryazdan, H. Hahn, Sliding wear-induced chemical nanolayering in Cu–Ag, and its implications for high wear resistance. *Acta Mater.* **72**, 148–158 (2014).
15. T. J. Rupert, C. A. Schuh, Sliding wear of nanocrystalline Ni–W: Structural evolution and the apparent breakdown of Archard scaling. *Acta Mater.* **58**, 4137–4148 (2010).
16. M. A. Meyers, A. Mishra, D. J. Benson, Mechanical properties of nanocrystalline materials. *Prog. Mater. Sci.* **51**, 427–556 (2006).
17. D. Shakhvorostov, K. Pohlmann, M. Scherge, Structure and mechanical properties of tribologically induced nanolayers. *Wear* **260**, 433–437 (2006).
18. D. Linsler, T. Schlarb, T. Weingartner, M. Scherge, Influence of subsurface microstructure on the running-in of an AlSi alloy. *Wear* **332–333**, 926–931 (2015).
19. P. Stoyanov, P. Stemmer, T. T. Järvi, R. Merz, P. A. Romero, M. Scherge, M. Kopnarski, M. Moseler, A. Fischer, M. Dienwiebel, Friction and wear mechanisms of tungsten–carbon systems: A comparison of dry and lubricated conditions. *ACS Appl. Mater. Interfaces* **5**, 6123–6135 (2013).
20. K. Kato, Wear in relation to friction—A review. *Wear* **241**, 151–157 (2000).
21. T. H. Fang, W. L. Li, N. R. Tao, K. Lu, Revealing extraordinary intrinsic tensile plasticity in gradient nano-grained copper. *Science* **331**, 1587–1590 (2011).
22. K. Lu, Making strong nanomaterials ductile with gradients. *Science* **345**, 1455–1456 (2014).
23. A. Mahato, Y. Guo, N. K. Sundaram, S. Chandrasekar, Surface folding in metals: A mechanism for delamination wear in sliding. *Proc. Math. Phys. Sci.* **470**, 14 (2014).
24. K. Zhang, J. R. Weertman, J. A. Eastman, Rapid stress-driven grain coarsening in nanocrystalline Cu at ambient and cryogenic temperatures. *Appl. Phys. Lett.* **87**, 061921 (2005).
25. T. J. Rupert, D. S. Gianola, Y. Gan, K. J. Hemker, Experimental observations of stress-driven grain boundary migration. *Science* **326**, 1686–1690 (2009).
26. D. Pan, S. Kuwano, T. Fujita, M. W. Chen, Ultra-large room-temperature compressive plasticity of a nanocrystalline metal. *Nano Lett.* **7**, 2108–2111 (2007).
27. R. Pippan, S. Scheriau, A. Taylor, M. Hafok, A. Hohenwarter, A. Bachmaier, Saturation of fragmentation during severe plastic deformation. *Annu. Rev. Mater. Res.* **40**, 319–343 (2010).
28. K. Lu, Stabilizing nanostructures in metals using grain and twin boundary architectures. *Nat. Rev. Mater.* **1**, 16019 (2016).
29. W. D. Nix, H. Gao, Indentation size effects in crystalline materials: A law for strain gradient plasticity. *J. Mech. Phys. Solids* **46**, 411–425 (1998).
30. B. Yao, Z. Han, K. Lu, Correlation between wear resistance and subsurface recrystallization structure in copper. *Wear* **294–295**, 438–445 (2012).
31. W. L. Li, N. R. Tao, K. Lu, Fabrication of a gradient nano-micro-structured surface layer on bulk copper by means of a surface mechanical grinding treatment. *Scr. Mater.* **59**, 546–549 (2008).
32. Y. S. Li, N. R. Tao, K. Lu, Microstructural evolution and nanostructure formation in copper during dynamic plastic deformation at cryogenic temperatures. *Acta Mater.* **56**, 230–241 (2008).

Acknowledgments: We thank J. Tan for assistance in the FIB experiments. **Funding:** We are grateful for the financial support of the Ministry of Science and Technology of China (grant 2012CB932201), the National Natural Science Foundation (grants 51231006 and 51261130091), and the Key Research Program of the Chinese Academy of Sciences (KGZD-EW-T06). **Author contributions:** K.L. initiated the investigation; X.C. prepared the samples and performed the experiments; X.C., Z.H., X.L., and K.L. analyzed the data and wrote the paper; K.L. and Z.H. supervised X.C. **Competing interests:** The authors declare that they have no competing interests. **Data and materials availability:** All data needed to evaluate the conclusions in the paper are present in the paper and/or the Supplementary Materials. Additional data related to this paper may be requested from the authors.

Submitted 16 August 2016
Accepted 8 November 2016
Published 9 December 2016
10.1126/sciadv.1601942

Citation: X. Chen, Z. Han, X. Li, K. Lu, Lowering coefficient of friction in Cu alloys with stable gradient nanostructures. *Sci. Adv.* **2**, e1601942 (2016).